Boscolo et al. *EPJ Techniques and Instrumentation* (2023) 10:16
https://doi.org/10.1140/epjti/s40485-023-00103-7

EPJ Techniques and
Instrumentation

RESEARCH ARTICLE **Open Access**

Mechanical model for the FCC-ee interaction region

Manuela Boscolo[1]*, Fabrizio Palla[2], Filippo Bosi[2], Francesco Fransesini[1] and Stefano Lauciani[1]

(Submitted to EPJ+ Techniques and Instrumentation special issue: Accelerating the design of the Future Circular Collider)

*Correspondence:
[1] INFN – Laboratori Nazionali di Frascati, Via Enrico Fermi, 54, 00044 Frascati RM, Italy
Full list of author information is available at the end of the article

Abstract

The Future Circular Collider FCC-ee aims at unprecedented luminosities to be obtained with the crab-waist collision scheme. In this paper we describe the mechanical model of the interaction region layout including its assembly procedure. After a discussion on the requirements and constraints, we present the engineered design of the vacuum chamber with the cooling system, the bellows, the vertex and outer tracker detectors and their integration in a carbon-fibre lightweight support structure that will support also the luminosity calorimeter.

PACS Codes: 29.20.db Storage rings and colliders

1 Introduction

The Future Collider FCC-ee is a design study of a high luminosity and high energy circular electron-positron collider with a proposed circumference of about 90.6 km, aiming to make precision studies and rare decay observations in the range between 91.2 (Z pole) and 365 GeV ($t\bar{t}$ threshold) centre-of-mass energy. Following the recommendations of the 2020 European Strategy for Particle Physics Update [1] the CERN Council has launched the FCC Feasibility Study in 2021, addressing technical aspects of the accelerator like the definition of the layout with the civil engineering and the related update on the cost estimate. This phase follows the publication of the first Conceptual Design Report (CDR) in 2019 [2–4] reporting the physics cases, the design of the lepton and hadron colliders, and the related technologies and infrastructures.

FCC-ee is conceived as double ring collider, with four interaction points (IPs), up to two radio-frequency system straights, and a tapering of the arc magnet strengths to match local energy. Figure 1 shows the latest layout where PA, PG, PD and PJ are the experiment sites, PH and PL the radio-frequency sites, PF the collimation section, and PB the injection/extraction section. The main changes with respect to the CDR layout are the eight access points, the four experimental sites instead of two, the reduced circumference of about 90.6 km (instead of 100 km). The optics of FCC-ee is designed to overlap the IPs of FCC-hh (an energy-frontier hadron collider). The IP transversely deviates from the layout

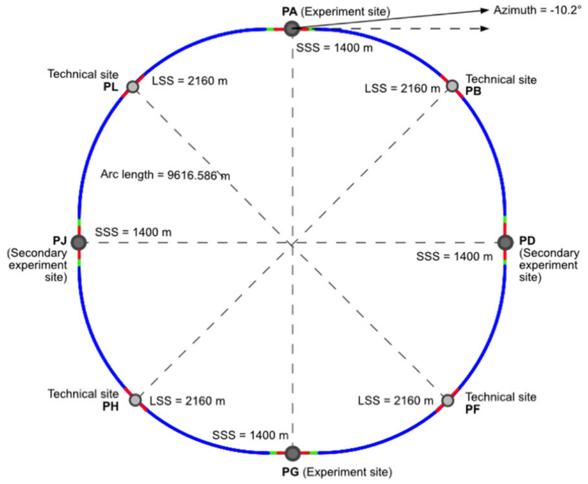

Figure 1 FCC-ee layout with 4 IPs (see text)

Table 1 Preliminary key parameters of FCC-ee IR as evolved from the CDR paramters, for scenarios with 4 IPs [5]

Circumference (km)	90.659
Crossing angle at IP (mrad)	30
ℓ^* (m)	2.2
SR power/beam (MW)	50

	Z	W	H	ttbar
Beam energy (GeV)	45.6	80	120	182.5
Luminosity/IP (10^{34} cm^{-2}s^{-1})	140	19.4	7.26	1.25
β_x^* (m)	0.11	0.2	0.3	1
β_y^* (mm)	0.7	1.0	1.0	1.6
ϵ_x (nm)	0.71	2.16	0.64	1.469
ϵ_y (pm)	1.40	4.32	1.29	2.98
Beam current (mA)	1270	135	26.7	5.0
Bunch number/beam (#)	15880	880	248	40
Bunch length by SR/BS (mm)	5.60/12.7	3.55/8.01	3.34/6.00	1.94/2.74
En. Spread σ_δ (SR) [%]	0.039	0.069	0.103	0.157
En. Spread σ_δ (BS) [%]	0.089	0.154	0.185	0.221

line by about 10.5 m outward. The booster has to bypass the FCC-ee detector at the IP for at least 8 m. Some of the FCC-ee interaction region (IR) beam parameters are listed in Table 1. The FCC-ee luminosity ranges from 2×10^{36} cm^{-2}s^{-1} per IP on the Z pole, to 1.25×10^{34} cm^{-2}s^{-1} per IP at the $t\bar{t}$ threshold. The Z pole run will be a high beam intensity operation mode, the top energy will be at low beam intensity to mitigate the beam emitted synchrotron radiation.

We discuss here the mechanical model of the central region of the FCC-ee Machine Detector Interface (MDI). The paper is organised as follows. Section 2 describes the constraints and requirements to the MDI design set by the accelerator and the detector. Section 3 describes the mechanical engineering design of the MDI with the details of the beam pipe and IR bellows. In Sect. 4 the tracker layout is detailed. Section 5 describes the luminosity calorimeter. Section 6 describes the support tube which will be used to integrate all the components described in the previous sections, together with the assembly sequence. Finally, in Sect. 7 we discuss the perspectives of this activity.

2 Requirements to the MDI design

The FCC-ee IR design is based on the crab-waist collision scheme, whose main ingredients to reach the high luminosity, are nano-beams at the IP, large crossing angle, and crab-waist sextupoles [6]. The MDI of the FCC-ee has a compact and complex design [7] that fulfils constraints given both by the machine and the detector requirements.

The FCC-ee optics varies with the beam energy so as to allow for a common IR layout at all energies. The flexibility of the IR optics is obtained by splitting the first quadrupole into three segments and by modulating their sign and strength according to the beam energy. Tens of nanometers in the vertical beam size and few microns horizontally require small β-functions at the IP, down to 0.1 m and 0.8 mm at the Z pole, that are obtained with a doublet of superconducting quadrupoles. The distance between the face of the final quadrupole to the IP (ℓ^*) is at 2.2 m from the IP, necessarily inside the detector. The beam lines in the IR are separated for the two beams, except for the common beam pipe over 1.8 m around the IP. There are no common quadrupoles in the IR.

In addition to the optics constraints to the IR layout, the physics reconstruction would benefit if the accelerator components were contained below a cone of 100 mrad from the IP along the z axis. To comply with these first requirements we have a compact MDI design with tight space constraints.

The crab-waist scheme requires a large horizontal crossing angle, set to 30 mrad. This value is obtained by strongly bending the outgoing beam trajectories from the IP so that the beams can successfully merge back close to the opposite ring [8], thus ensuring that most of the locally generated synchrotron radiation (SR) does not strike the IR central beam pipe. This solution for FCC-ee meets the requirement derived from the LEP2 experience, where manageable detector backgrounds were found with a critical energy of 72 keV from 260 m from the IP [9]. In fact, the critical energy of the SR from bending magnets are below 100 keV from 500 m upstream the IP for the incoming beam, and the last upstream dipole is located at least 100 m from the IP.

One of the beam optics challenges for the collider is to provide an adequate dynamic aperture with such small β-functions at the IP. These values, together with a small ℓ^*, lead to a high vertical chromaticity around the IP, that is corrected locally by two sextupole magnets. At the $t\bar{t}$ energy a wide momentum acceptance is required to cope with the beamstrahlung emitted at collision.

The detector solenoid field is 2 T at the IP (being a cylinder with a half-length of about 5 m and a diameter of around 3.8 m), and a compensation solenoid placed at 1.23 m from the IP cancels the $\int B_z\, dz$ between the IP and the faces of the final quadrupole. This value poses a challenge to the design of the first final focus quadrupole, QC1, in that the distance between the magnetic centres of the two beams is only a few centimetres.

A screening solenoid is placed around the final focus quadrupoles to produce an opposite field to that of the detector, thereby cancelling the detector field. Figure 2 shows the IR layout in an expanded vertical scale [10] with 10 mm radius of the central beam pipe.

In order to profit of the small beam pipe radius, the vertex detector (see Sect. 4.1) must be placed at the smallest affordable distance from it, its angular coverage of $|\cos(\theta)| < 0.99$ as well as a lightweight mechanical structure.

In order to avoid any material in front of the luminosity calorimeter (see Sect. 5) all other detector elements must be placed above 110 mrad with respect to the beam line.

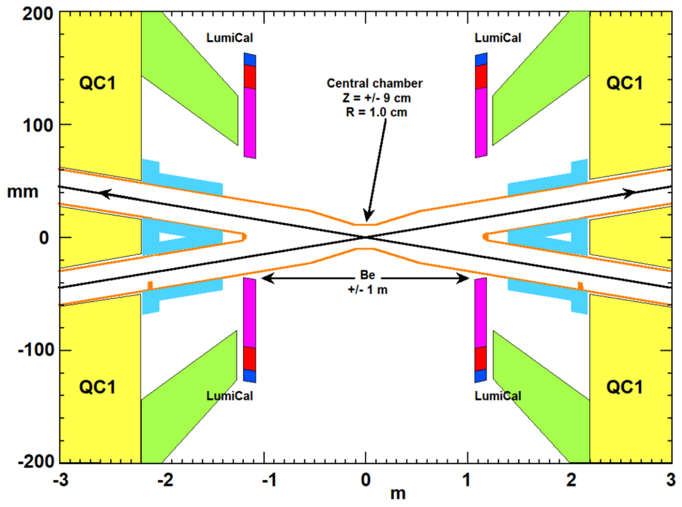

Figure 2 IR layout in an expanded vertical scale with 10 mm radius of the central beam pipe [10]

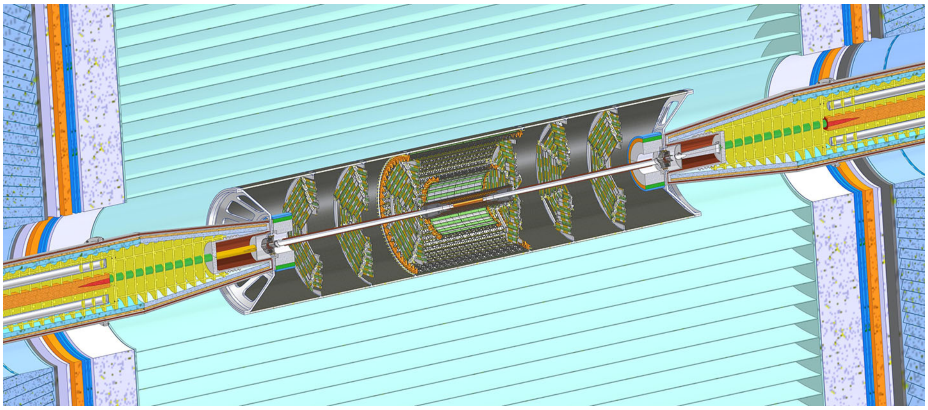

Figure 3 Section of the MDI CAD model for about ±1.5 m from the interaction point in the IDEA detector. The beam pipe, the luminosity monitor, the vertex and outer trackers, will all be supported by the support tube shown here with its endcaps

3 MDI engineering design

We describe here the mechanical model of the very central region, as shown in Fig. 3. Figure 4 shows a larger view that goes through the compensation solenoid and the first final focus quadrupole surrounded by its screening solenoids. It is a compact design, also due to the requirement of being inside a small cone of 100 mrad. This tight constraint might be slightly increased once the superconducting IR magnets and their cryostats will be engineered and integrated with this model. We also note that the detector will be about 5 m long, so the elements in Fig. 4 will be almost completely inside the detector.

All the components will be mounted inside a lightweight carbon-fibre support tube, that has been developed to ease the integration of the different detector and machine parts, into a single rigid structure shown in Fig. 3. This latter component will be described in detail in Sect. 6, together with the assembly procedure for all components of the MDI region.

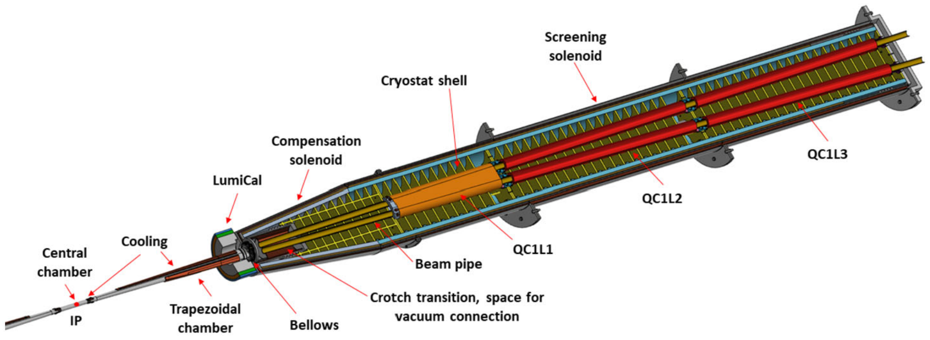

Figure 4 Section view of the accelerator components from the IP to the end of the first final focus quadrupole (QC1), at about 8.4 m

Table 2 Composition of the central chamber wall

	Thickness [mm]	Material	X/X_0 (%)
	0.005	Gold	0.15
	0.35	AlBeMet162	0.14
	1	Paraffin	0.18
	0.35	AlBeMet162	0.14
Total	**1.705**		**0.61**

Figure 5 Central chamber in AlBeMet162 including cooling inlets and outlets for the Paraffin cooling circuit housed in a double layer, 180 mm long

3.1 Mechanical model of the beam pipe

The mechanical model of the IR vacuum chamber has to fulfill conflicting requirements: it must have a smooth shape to provide low impedance, it has to be as thin as possible to minimize the material budget as required by the physics performance and at the same time rigid enough to resist stresses, it has to be cooled to control the beam heat loads and possible losses and heat due to synchrotron radiation.

The impedance was minimised by carefully designing the transverse section of the beam pipe, with a smooth transition from a circular to an elliptical transverse shape, as discussed in Refs. [10, 11]. The central chamber extends for ±90 mm from the IP. It will be composed by a double layer of AlBeMet162 with liquid cooling inside through a copper inlet and outlet channel system, as shown in Fig. 5. The double layer structure is made of two concentric cylinders, each with a thickness of 0.35 mm and assembled with 1 mm gap for the paraffin flow. This brings the effective diameter of the central beam pipe and its cooling layer to 23.4 mm.

The AlBeMet162 is an alloy of 62% of beryllium and 38% of aliminium; it has been chosen for its high modulus and low-density characteristics with the fabrication and mechanical properties characteristics of the aluminium. The cooling channels will be in copper, and they will be embedded on the AlBeMet162 by using the additive technique called *thick copper deposition*. The section of the beam pipe smoothly changes from a circular shape

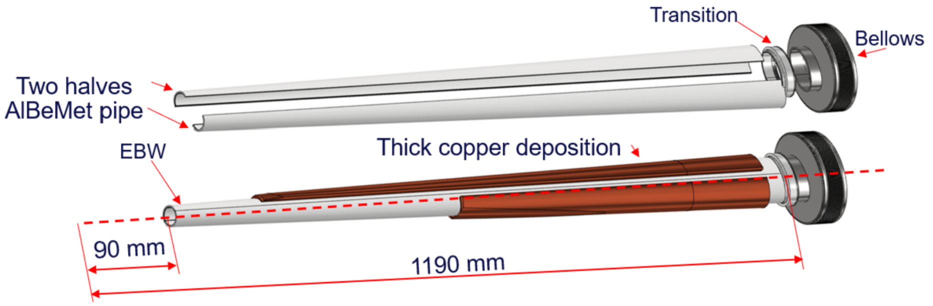

Figure 6 AlBeMet162 vacuum chamber from 90 mm from the IP to the bellows, named trapezoidal chamber for its shape, with asymmetrical copper cooling channels

Table 3 Liquid cooling properties for paraffin and water, used as input for the thermo-structural analysis of the vacuum chamber

	Paraffin	Water
Flow rate [kg/s]	0.015	0.0019
Section [mm^2]	68.17	9.62
Velocity [m/s]	0.3	0.2
Inlet temperature [°C]	18	18
Convective coefficient [W/m^2K]	900	1200

to an elliptical shape. The central chamber is merged with two symmetric beam pipes with 15 mm radius at 1.28 m from the IP.

The geometry is optimized to minimize the material budget and to guarantee a proper coolant flow to remove the heat generated by wakefields; the thickness of 0.35 mm of AlBeMet162 is the minimum limit for the mechanical resistance.

The vacuum chamber starting from 90 mm from the IP to the bellows is shown in Fig. 6, and is called *trapezoidal chamber*. After a short transition from the central chamber, the thickness of the trapezoidal chamber remains to a constant value of 2 mm. It will be in AlBeMet162 as for the central pipe. For this region the AlBeMet162 pipe will not be in a double layer to provide the necessary cooling, but there will be copper cooling channels deposited on the AlBeMet162 with the same *thick copper deposition* technique described for the central chamber. In this case the cooling channels on the beam pipe will be asymmetric, as shown in Fig. 6 to allow for the required acceptance of the luminosity calorimeter. A cone of 50 mrad was used as the cutting profile.

The vertex tracker detector, described in Sect. 4, will be mounted on top of the trapezoidal chamber.

A thermo-structural analysis has been performed to calculate the temperature distribution, stress, strain and displacement, using the characteristics for paraffin and water flow reported in Table 3 as input.

The temperature distribution for the two chambers is shown in Fig. 7, where about 50 W of deposited power was assumed over the central chamber and 130 W over the trapezoidal chamber, and in case of a perfect thermal contact between the materials. This study [12] shows that with paraffin as liquid coolant the maximum temperature of the central chamber will be 33.1 °C, and 47.6 °C for the trapezoidal chamber cooled with water. The paraffin will reach 20.1 °C, and the water 20.5 °C, respectively. This cooling system can

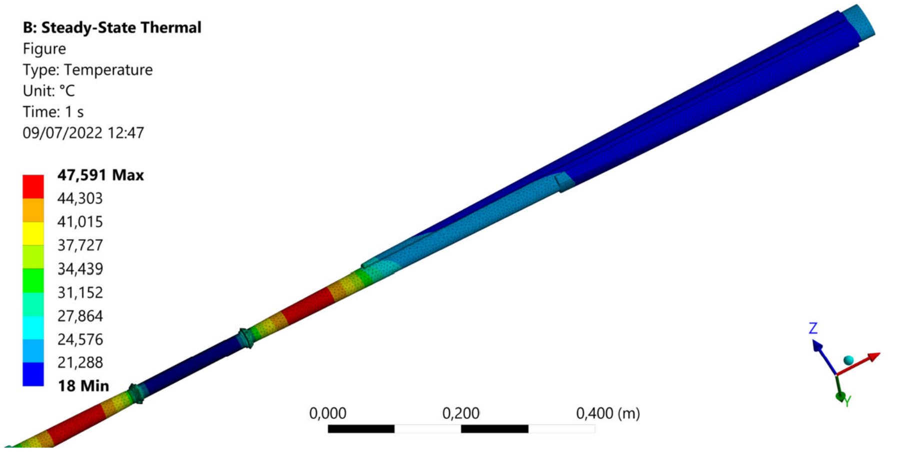

Figure 7 ANSYS [13] simulation of the temperature distribution along the trapezoidal chamber for about 50 W of deposited power over the central chamber and 130 W over the trapezoidal chamber

Table 4 Structural analysis in two constraint configurations

Case	Maximum stress Von Mises [MPa]	Maximum displacement [mm]
Fixed ends	46	0.01
Cantilevered, Simply supported	25	0.3

tolerate an increase of about 15% of heat load, to sustain higher values it will be necessary to adapt the velocity and flow rate of the coolant flow.

We have performed the structural analysis of the vacuum chamber and estimated its maximum stress and displacement for two constraint configurations: fixed ends or cantilevered-simply support. For this study we considered the earth gravity, the vacuum load and we assumed the vertex detector attached to the chamber; we have also used the temperature distribution along the chamber as input. Results are summarised in Table 4. The stresses and strains are acceptable; the estimated safety factor is about 5, considering that the yield strength of AlBeMet162 is 193 MPa. In any case the buckling behaviour is more critical than the static one, therefore some experimental tests would be extremely useful to check our analysis.

3.2 Mechanical model of the IR bellows

At either ends of the trapezoidal chamber there will be bellows to absorb chamber-to-chamber misalignments, and thermal expansions of the order of few millimeters. The IR bellows has to be as compact as possible due to the small space available, which is about 70 mm longitudinally. We discuss here how the proposed design of the bellows fits with our mechanical requirements.

The bellows will be attached on one side to the trapezoidal chamber, on the other side to the remote vacuum flange, close to the superconducting IR magnet system, which will be embedded in a cryostat. For the moment we considered only the elongation due to the thermal expansion given by beam heat load and that due to the assembly. Two slightly different bellows geometries are proposed at each IP side to isolate the central chamber from external stresses and strain due to assembly and operation conditions. They will have the same axial length and the same RF contacts configuration, but with a different configu-

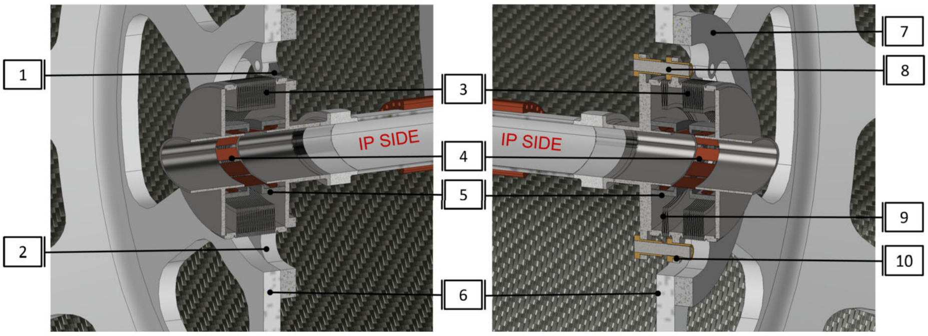

Figure 8 Left: *single bellow*; right: *double bellows*. The elements of the bellows shown in the pictures are: (**1**) Convolutions; (**2**) RF blade; (**3**) Support tube endcap; (**4**) Bellows flange; (**5**) Blades pusher; (**6**) Endcap-bellows flange

ration, maintaining a symmetrical geometry. The study of the electromagnetic forces on the magnets in case of accidental quench has not been performed yet. This will give an additional specification to the possible elongation of the bellows.

Since bellows can create a resonant cavity and lead to vacuum, stability and overheating problems, any geometrical discontinuity has to be avoided and electrical contact must be preserved. An adaptation of ESRF bellows design [14] has been considered as a starting point for our design. There are twelve CuBe blades lying around elliptical shape of vacuum chamber and the desired electrical contact is obtained by a blade pusher.

The first bellows, named *single bellows*, is shown in Fig. 8 (left). It is properly anchored to the endcap of the support tube with a flange that will allow to align the beam pipe inside it. On the side toward the cryostat the bellows has convolutions to mitigate the thermal expansions that also provide the proper clearance during the assembly and the connection between the remote vacuum connection and the vacuum chamber.

The second bellows, named *double bellows* and shown Fig. 8 (right) is a bellows with the same envelopes and dimension of the *single bellows* to keep a symmetrical geometry but with two set of convolutions, thus allowing to isolate the IR beam pipe from stress and strain coming from the assembly procedure and during the operation, i.e. thermal expansion, and to preserve the thin walled central chamber. On the side toward the IP the bellows is made up of few convolutions to absorb the thermal expansion of the IR beam pipe; a linear bearing system is used to allow only an axial degree of freedom. On the cryostat side the bellows has more convolutions to provide suitable clearance for the assembly. An intermediate flange is present and anchored to the support tube endcap.

The wakefields calculations to evaluate the impedance budget for these bellows are in progress with the simulation code CST [15] and are not subject of this paper.

4 Silicon tracker layout

Two detector concepts for the FCC-ee detectors were described in the CDR [2–4]: CLD, based on the work done for a detector for the CLIC collider, and IDEA, possibly more cost effective. The one presented here for this study is an evolution of the IDEA concept.

The Silicon Tracker of IDEA features two main subsystems:

- a vertex detector, located closer to the beam pipe, between 13.7 and 34 mm, covering an angular acceptance of about $|\cos(\theta)| < 0.99$, made of MAPS detectors;

- an outer tracker, located at a larger radius between 11.2 and 31.5 cm, composed of a barrel section and forward disks, made of MAPS silicon pixel detectors.

The current design is based on technology already installed or envisaged for the main experiments upgrades (like Belle II or ATLAS). It is meant to be a realistic estimate, although engineered, of a tracker fulfilling the acceptance and material budget requirements, which can be integrated with the rest of the machine elements. Future designs, especially of the vertex detectors using other technologies will require new integration studies.

4.1 Vertex detector

The vertex detector is composed of three barrel concentric layers.

The elementary unit is a module of dimensions $32(z) \times 8.4(r-\phi)$ mm^2. Each module has two chips abutted in z inspired from the ARCADIA INFN R&D [16]. The active area is made of $640(z) \times 256(r-\phi)$ pixels of 25×25 μm^2 size.

A total of 2 mm inactive space in $r-\phi$ is envisaged, also containing the chip periphery. The sensor thickness of the modules is 50 μm (0.052X/X$_0$) and their power consumption is assumed to be 50 mW/cm^2.

4.1.1 Vertex detector mechanical structure

The modules are mounted on a carbon fibre structure that comprises three barrel layers.

In order to allow 2 mm radial clearance for its insertion, and given that the central beam pipe and its cooling blanket has a diameter of 23.4 mm, the first layer is located at a radius of 13.7 mm. Its length is constrained by the central beam pipe cooling manifolds. The first layer comprises 15 staves of 6 modules each along z; the staves are overlapped in ϕ, as shown in Fig. 9, to allow for internal alignment.

A lightweight support on each ladder provides rigidity and allows the mounting of the MAPS. The structure is made of thin carbon fibre walls interleaved with Rohacell, which holds the sensors (facing the beamline), which in turn support two buses (one for data and another for the power) 1.8 mm wide each per side. The thickness of the bus comprises 200 μm kapton and 50 μm aluminum for a total of 0.09 X/X$_0$. The ladders are arranged on a pinwheel geometry.

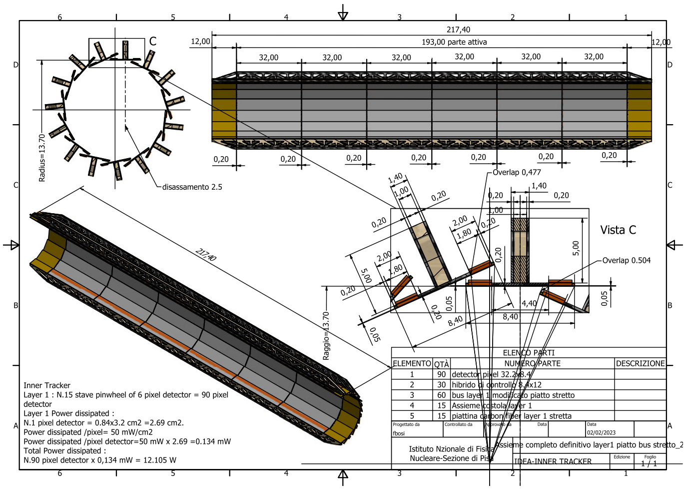

Figure 9 Layer 1 layout of the vertex detector

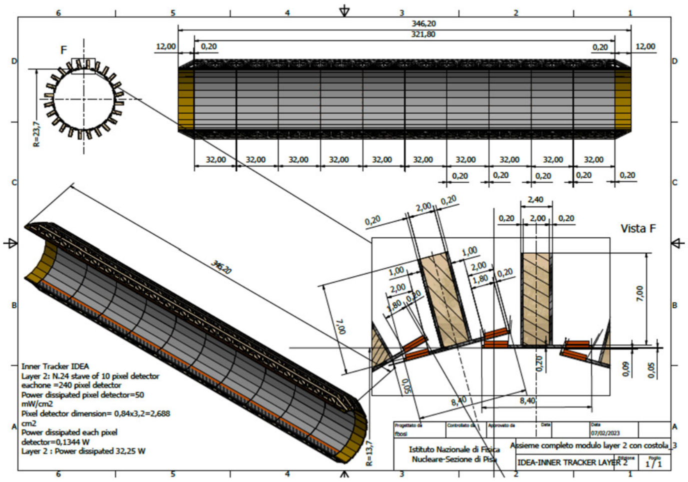

Figure 10 Layer 2 layout of the vertex detector

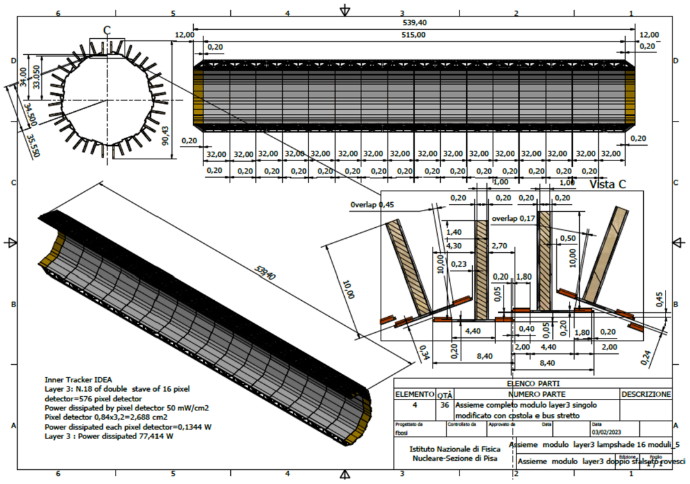

Figure 11 Layer 3 layout of the vertex detector

The second layer, with a similar structure of the first one, is made of 24 ladders of 10 modules each, at an average radius of 23.7 mm, and is shown in Fig. 10. The orientation of the angle of the wheel is opposite to the one of the first layer, in order to mitigate any possible charge dependent effects on the tracks reconstruction.

The 18 ladders that compose the third layer are arranged in a lampshade fashion, which is symmetric in azimuth; each one is composed of double overlapping detectors rows consisting of 16 modules, as shown in Fig. 11. The ladders are located at 33.05 mm and 35.55 mm radial positions.

The vertex layers are mounted on a carbon fibre conical support, whose angular coverage ranges between 116 and 141 mrad, as shown in Fig. 12, that is then anchored to trapezoidal beam pipe, leaving a clearance with the central beam pipe inlets and outlets manifolds of 200 μm. The total weight of the conical support is about 450 grams.

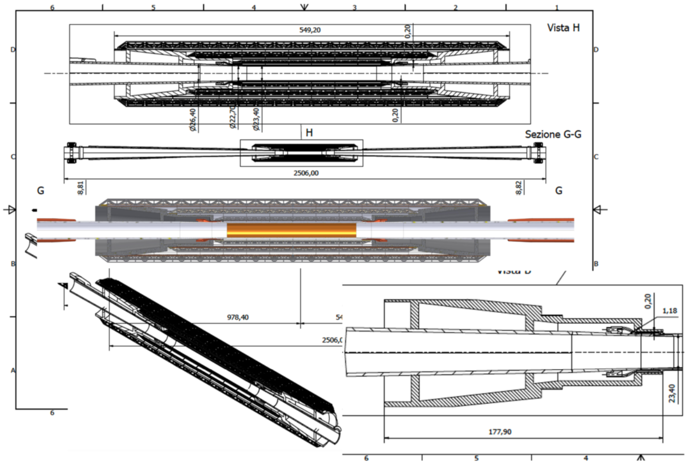

Figure 12 Vertex detector as mounted on the beam pipe, with its rendering in the central color picture. The bottom right drawing shows the conical vertex support structure mounted on the trapezoidal beam pipe

Table 5 Power dissipated, weight and material budget for the vertex detector layers

Layer No.	Radius [mm]	Power [W]	Mass [g]	X/X_0(%)
1	13.7	12.1	19.1	0.25
2	23.7	32.7	60.9	0.25
3	33.05–35.55	77.5	159.7	0.25

The power dissipated by each layer as well as its weight and material budget is reported in Table 5. The entire structure will be cooled by air, which passes through channels embedded in the conical carbon fibre support structure.

4.2 Outer tracker

The outer tracker detector is composed of two barrel layers and three disks on either sides of the IP.

The elementary unit is a module of dimensions $40.6(z) \times 42.2(r-\phi)$ mm^2. Each module has four hybrid pixels inspired by the ATLAS PIX3 R&D [17]. The active area of the chip consists of 132 columns of 372 pixels each, with squared pixel of 50 μm side. The sensor thickness of the modules is 50 μm and their power consumption is assumed to be 100 mW/cm^2.

The same module type is being used for the barrel layers and the disks, although this poses some problems in the optimisation of the layout. In a further iteration we will consider modules better suited for the disks, but this kind of exercise goes beyond the current scope.

One barrel layer is placed at 13 cm (Middle barrel) and is made of 22 ladders, each with 8 modules, as shown in Fig. 13. The outermost layer (Outer barrel) is placed at 31.5 cm and is composed of 51 ladders of 16 modules each, as shown in Fig. 14. The outer layer is supported by a flange that is attached to the external support tube. The flange also supports the Middle barrel as well as the first disks (see later).

The modules are placed on top of a lightweight triangular truss structure. The staves are mechanical structures holding the modules. The detail of the cross section of a stave for the Outer barrel is shown in Fig. 15. It is composed of a carbon fibre multilayered structure,

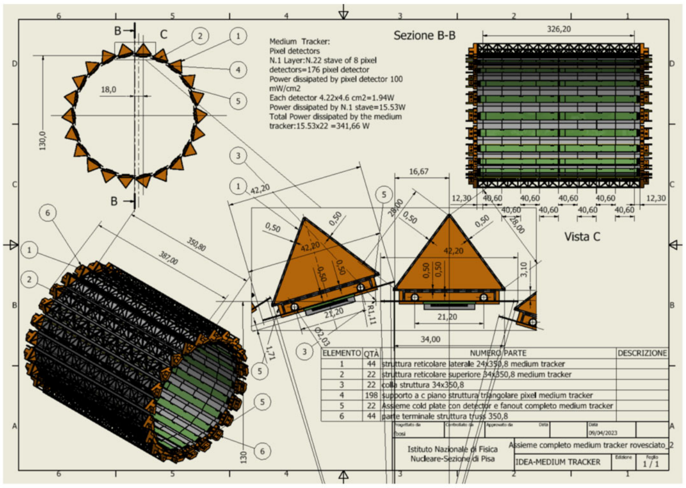

Medium Tracker:
Pixel detectors
N.1 Layer:N.22 stave of 8 pixel detectors=176 pixel detector
Power dissipated by pixel detector 100 mW/cm2
Each detector 4.22x4.6 cm2=1.94W
Power dissipated by N.1 stave=15.53W
Total Power dissipated by the medium tracker:15.53x22 =341,66 W

ELEMENTO	QTÀ	NUMERO PARTE	DESCRIZIONE
1	44	struttura reticolare laterale 24x350,8 medium tracker	
2	22	struttura reticolare superiore 34x350,8 medium tracker	
3	22	colla struttura 34x350,8	
4	198	supporto a c piano struttura triangolare pixel medium tracker	
5	22	Assieme cold plate con detector e fanout completo medium tracker	
6	44	parte terminale struttura truss 350,8	

Figure 13 Layout of the Middle barrel layer

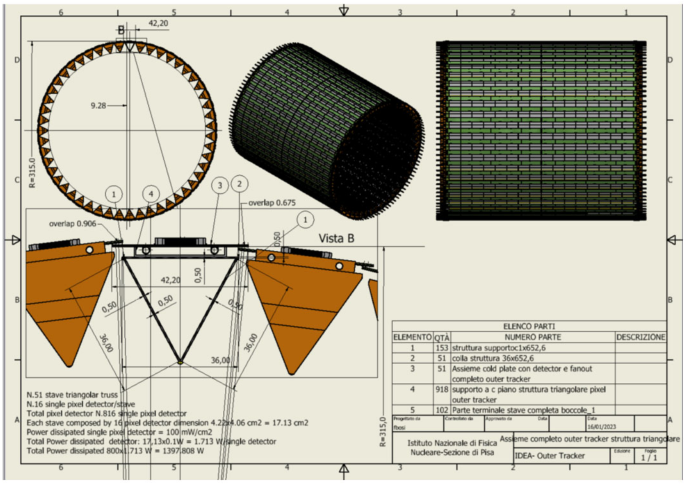

N.51 stave triangolar truss
N.16 single pixel detector/stave
Total pixel detector N.816 single pixel detector
Each stave composed by 16 pixel detector dimension 4.22x4.06 cm2 = 17.13 cm2
Power dissipated single pixel detector = 100 mW/cm2
Total Power dissipated detector: 17,13x0.1W = 1.713 W/single detector
Total Power dissipated 800x1.713 W = 1397.808 W

ELENCO PARTI

ELEMENTO	QTÀ	NUMERO PARTE	DESCRIZIONE
1	153	struttura supportoc1x652,6	
2	51	colla struttura 36x652,6	
3	51	Assieme cold plate con detector e fanout completo outer tracker	
4	918	supporto a c piano struttura triangolare pixel outer tracker	
5	102	Parte terminale stave completa boccole_1	

Figure 14 Layout of the Outer barrel layer

comprising 120 μm thick carbon fibre KDU13, and two carbon fleeces of 65 μm in total, to support two polymide tubes of 2.2 mm diameter and 90 μm thick, in which demineralised water will be circulating.

An electronic bus, bringing the power distribution and the readout and control signals is running for the entire stave length, and is put on top of the modules. It is terminated at the end of both sides of the stave by an hybrid circuit.

Three disks per each side, located at $z = \pm 30.47$, ± 62 and ± 93 cm, complete the outer tracker. The inner disk is located inside the barrel and extends from an innermost radius of 3.45 cm to an outer radius of 27.5 cm. The other two pairs of disks have an inner radius of 7 and 10.5 cm, and extend up to a radius of 28.5 cm to allow an hermetic coverage.

Each disk is composed of four front and backward petals, made of the modules of the same type of those of the barrels. The support structure of each disk is made of a sandwich

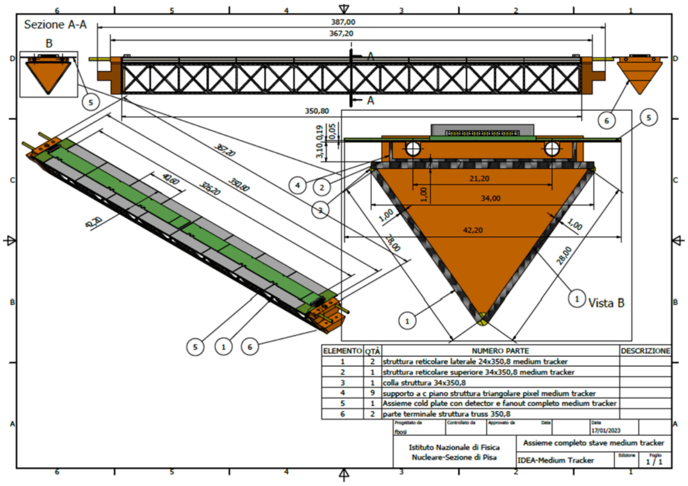

ELEMENTO	QTÀ	NUMERO PARTE	DESCRIZIONE
1	2	struttura reticolare laterale 24x350,8 medium tracker	
2	1	struttura reticolare superiore 34x350,8 medium tracker	
3	1	colla struttura 34x350,8	
4	9	supporto a c piano struttura triangolare pixel medium tracker	
5	1	Assieme cold plate con detector e fanout completo medium tracker	
6	2	parte terminale struttura truss 350,8	

Progettato da fbosi
Controllato da
Approvato da
Data
Data 17/01/2023
Istituto Nazionale di Fisica Nucleare-Sezione di Pisa
Assieme completo stave medium tracker
IDEA-Medium Tracker
Edizione
Foglio 1 / 1

Figure 15 Stave cross-section for the Middle barrel

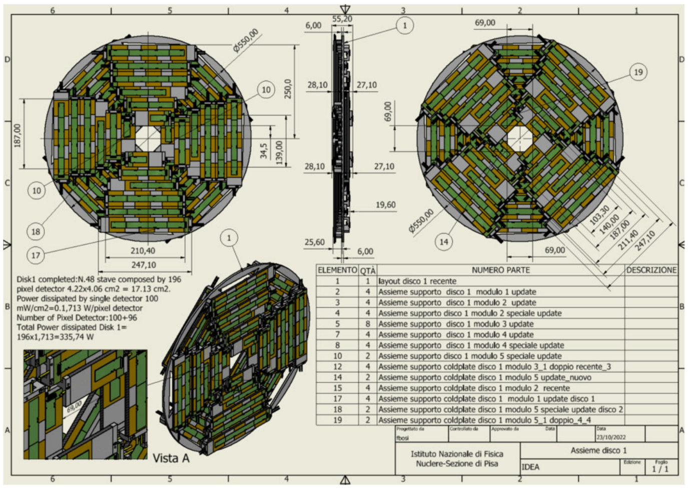

Disk1 completed:N.48 stave composed by 196 pixel detector 4.22x4.06 cm2 = 17.13 cm2.
Power dissipated by single detector 100 mW/cm2=0.1,713 W/pixel detector
Number of Pixel Detector:100+96
Total Power dissipated Disk 1= 196x1,713=335,74 W

ELEMENTO	QTÀ	NUMERO PARTE	DESCRIZIONE
1	1	layout disco 1 recente	
2	4	Assieme supporto disco 1 modulo 1 update	
3	4	Assieme supporto disco 1 modulo 2 update	
4	4	Assieme supporto disco 1 modulo 2 speciale update	
5	8	Assieme supporto disco 1 modulo 3 update	
7	4	Assieme supporto disco 1 modulo 4 update	
8	4	Assieme supporto disco 1 modulo 4 speciale update	
10	2	Assieme supporto disco 1 modulo 5 speciale update	
12	4	Assieme supporto coldplate disco 1 modulo 3_1 doppio recente_3	
14	2	Assieme supporto coldplate disco 1 modulo 5 update_nuovo	
15	4	Assieme supporto coldplate disco 1 modulo 2 recente	
17	4	Assieme supporto coldplate disco 1 modulo 1 update disco 1	
18	2	Assieme supporto coldplate disco 1 modulo 5 speciale update disco 2	
19	2	Assieme supporto coldplate disco 1 modulo 5_1 doppio_4_4	

Progettato da fbosi
Controllato da
Approvato da
Data
Data 23/10/2022
Istituto Nazionale di Fisica Nuclere-Sezione di Pisa
Assieme disco 1
IDEA
Edizione
Foglio 1 / 1

Figure 16 Layout of the first disk

of thin carbon fibre walls (each of 0.3 mm thickness) interleaved with Rohacell (5.4 mm thick).

A sketch of the first disk is shown in Fig. 16.

The power dissipated by each barrel layer and disk as well as the weight in the detector area is reported in Table 6. Preliminary computations indicate that the largest temperature variation between the coolest point (below the pipe) and the chip periphery is about 7 K.

5 Luminosity calorimeter

The FCC-ee luminosity calorimeter [18] is composed of two cylindrical devices, placed at about 1 meter away from the IP. The calorimeter is composed of a multilayered active structure, in which 26 passive tungsten circular disks, each of 3.5 mm thickness, are interleaved with 25 silicon pad detectors, in a 1 mm housing.

Table 6 Power dissipated and weight for each one of the barrel layers and disks of the Outer tracker

Part	Power [W]	Mass [g]
Middle Barrel	342	1040
Outer Barrel	1370	3696
Disk 1	336	845
Disk 2	425	1193
Disk 3	370	1054

The physical dimensions of each calorimeter span a sensitive radial coverage between 54 and 115 mm from the beamline and a service region, ranging from 115 to 145 mm, where the electronic readout, cables and cooling are placed.

The front face of the calorimeter (the first tungsten disk) is located at 1074 mm from the interaction point.

The total weight of the calorimeter is about 65 kg per each side.

In order to measure the luminosity with an accuracy of the order of 10^{-4} the calorimeter has a stringent requirement on the knowledge of its boundaries. in particular:

- its inner radius needs to be defined with a precision of $\pm 1.5\ \mu$m;
- its outer radius needs to be defined with a precision of $\pm 3.5\ \mu$m;
- the relative positioning of the two sides needs to be known with a precision of $\pm 110\ \mu$m.

The tungsten disks and the silicon pads must be assembled as single-piece parts, in order to fulfill the requirements of the very accurate positioning: once assembled, the calorimeter is a rigid hollow cylinder.

To avoid interference with the bellows and preserve the calorimeter integrity, it is proposed that the last four detector layers have a inner radius 2 cm larger than the others, as it is shown in Fig. 17. The impact of this solution on the physics performance is currently under evaluation, but it is expected to be marginal.

6 The support tube and the MDI assembly strategy

6.1 IR carbon-fibre support tube

This section describes a novel concept for the FCC-ee MDI, the support tube, that has been developed to ease the integration of the accelerator and detector components into a single rigid structure. In particular, this structure will allow to provide a cantilevered support for the pipe, it will avoid loads on thin-walled central chamber during assembly, and it will support the LumiCal and the outer tracker. The support tube is an empty cylindrical structure made with a multiple layer structure, composed as described in Table 7.

This support tube is longitudinally split in two halves, it is complemented by two aluminium flanges, and by two endcaps that will support the LumiCal and the beam pipe. Six aluminum ribs are fixed inside the tube in order to support the outer tracker. It will be introduced inside the detector thanks to longitudinal rails fixed to its external surface.

A structural analysis has been performed to calculate the stress and displacement in each part of the support tube, namely the reinforcement, carbon-fibre, and the honeycomb. The double fixed ends case has been considered as constraint configuration. The loads that have been considered are listed in Table 8.

The analysis was performed using overestimated values, which take into account estimated weights of the additional services material (such as the water ducts and the power

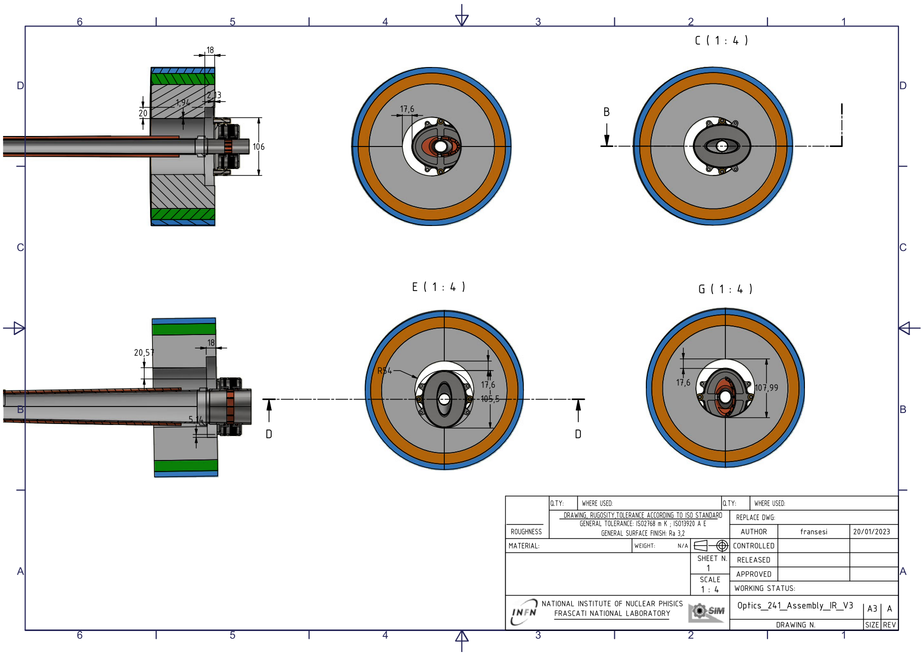

Figure 17 Luminosity calorimeter and bellows details

Table 7 Composition of the multiple layers structure

Thickness [mm]	Material	Orientation
0.25	Epoxy carbon woven (230 MPa)	45
0.25	Epoxy carbon woven (230 MPa)	–45
0.25	Epoxy carbon woven (230 MPa)	45
0.25	Epoxy carbon woven (230 MPa)	–45
4	Honeycomb	0
0.25	Epoxy carbon woven (230 MPa)	–45
0.25	Epoxy carbon woven (230 MPa)	45
0.25	Epoxy carbon woven (230 MPa)	–45
0.25	Epoxy carbon woven (230 MPa)	45

Table 8 Loads considered over the support tube for the structural resistance analysis. For the disks, middle and outer barrel a safety margin of a factor 3 has been considered to account for the services

Component	Value [kg]
Vacuum Chamber	51
LumiCal	2 × 70
Disks	18
Middle Barrel	3
Outer Barrel	11

cables that run from the detection region to the end of the support tube) finding that the structural resistance is safely respected.

The results of the analysis are summarized in Table 9, they show the small stress and displacement values.

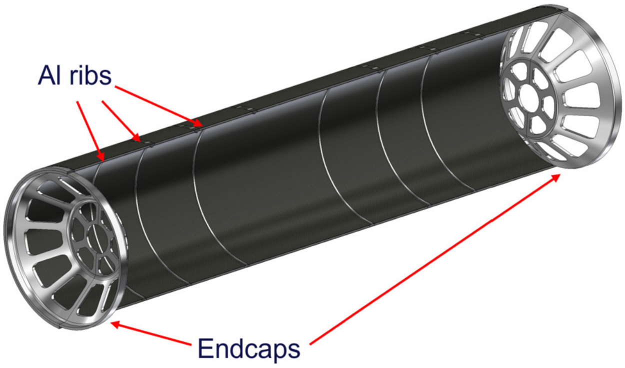

Figure 18 Carbon-fibre cylindrical support tube

Table 9 Structural analysis of the support tube, results of the maximum stress and maximum displacement

Support tube	Maximum stress [MPa]	Maximum displacement [μm]
Aluminium flanges	2.70	13
Aluminium ribs	0.09	14
Honeycomb	0.001	15
Carbon fiber	0.30	15

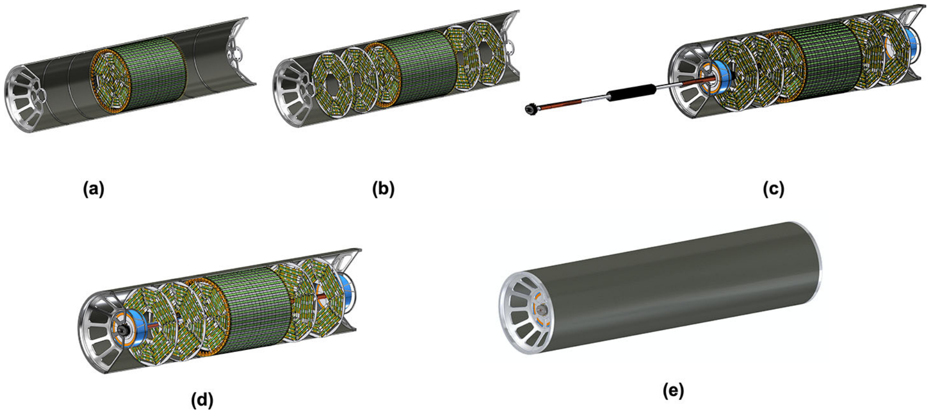

Figure 19 MDI assembly sequence

6.2 Assembly sequence and alignment

Thanks to the design of the support cylinder, the assembly of the entire system can be implemented in a modular way allowing a careful alignment of all the MDI components. The mounting precision of the detector elements will be better than 100 μm, and will be maintained during assembly, using dedicated tools. Once in place, the main structures will be surveyed with an accuracy of about 50 μm using laser scanner technology, like the one in [19].

The assembly sequence has been careful studied and is schematically described in Fig. 19. We do plan to model the assembly sequence both with CAD as well as with dedicated tools using a mock-up of all components.

One of the two halves of the cylinder is taken as a base for the mounting the detector components and the vacuum chamber. It will be mounted on a cradle which will sustain it rigidly.

The first step consists of assembling the Outer Barrel, the Middle Barrel and the innermost disks (disks 1) as a single mechanical structure in the laboratory. This assembly will then be fixed to the half cylinder (a). Successively, the other disks will be positioned and installed over the reinforcement ribs of the support tube (b).

After the positioning of the Outer tracker parts, the LumiCal will be mounted in a centered position on the endcaps of the support tube, and it will then be fixed to it (c).

The vacuum chamber, together with the vertex detector mounted on top, will be then slid inside, using a dedicated tool, and the Lumical can be aligned in its final position (d).

Finally, the second half of the support tube will be installed, concluding the assembly procedure (e).

7 Perspectives and outlook

The MDI design is complex and challenging, due to the demanding performances of the FCC-ee collider and the detector.

This paper presented the mechanical model of the central interaction region, including the mechanical design of the beam pipe with its cooling system along with the other components present in the area: the luminosity calorimeter, the IR bellows, and the IDEA silicon tracker detectors.

The support tube concept has been introduced for the first time, that will support all the aforementioned components inside. It will be a lightweight carbon-fibre tube attached to the IDEA drift chamber. Similar integration study will be performed for the CLD. For this support tube we presented here also the structural simulations.

We will finalize the design of the IR bellows according to the ongoing wakefields simulations, we will design the remote flange to be attached close to the IR bellows. Further progress will be achieved by advances on the engineering of the superconducting IR magnets and their cryostats, as well as on the definition of the interface with the main detector. The alignment system of the MDI, not mentioned here, will have to be integrated in the design, as well as all the supports, services, etc. Ongoing studies show that three-dimensional positions accuracy of the order of 5 μm or better could be achievable with optical fibres [20].

We have recently proposed a full-scale mock-up with prototyping of some components to complement the 3D CAD model and FEM simulations. In particular, few prototypes of the vacuum chamber with the cooling system, the IR bellows, the carbon-fibre support tube, and tests on the air cooling of the vertex detector will give an experimental validation of these key components described in this paper.

Acknowledgements

The authors would like to thank the colleagues from the MDI group for useful discussions, in particular Mogens Dam for the luminosity monitor, Alexander Novokhatski for the heat load estimates and impedance calculations, Michael Koratzinos for the conceptual design of the IR magnets, and Luigi Pellegrino on the mechanical model. We also warmly thank Frank Zimmermann and Michael Benedikt for their continuous support and encouragement to the effort on the MDI study.

Funding

This work was partially supported by the European Union's Horizon 2020 research and innovation programme under grant No 951754 – FCCIS Project, and by INFN.

Availability of data and materials

The datasets used and/or analysed during the current study are available from the corresponding author on request.

Declarations

Ethics approval and consent to participate

Not applicable.

Consent for publication

The authors declare that they have obtained the consent from their institutions to publish the article.

Competing interests

The authors declare that they have no competing interests.

Author contributions

All authors read and approved the final manuscript.

Author details

[1]INFN – Laboratori Nazionali di Frascati, Via Enrico Fermi, 54, 00044 Frascati RM, Italy. [2]INFN Sezione di Pisa, Largo Bruno Pontecorvo, 3, 56127 Pisa, Italy.

Received: 17 March 2023 Accepted: 28 May 2023

References

1. European Strategy Group. 2020 Update of the European Strategy for Particle Physics. 2020. CERN-ESU-015.
2. Abada A, et al. FCC physics opportunities: future circular collider conceptual design report volume 1. Eur Phys J C. 2019;79(6):474. https://doi.org/10.1140/epjc/s10052-019-6904-3.
3. Abada A, et al. FCC-ee: the lepton collider: future circular collider conceptual design report volume 2. Eur Phys J Spec Top. 2019;228(2):261–623. https://doi.org/10.1140/epjst/e2019-900045-4.
4. Abada A, et al. FCC-hh: the hadron collider: future circular collider conceptual design report volume 3. Eur Phys J Spec Top. 2019;228(4):755–1107. https://doi.org/10.1140/epjst/e2019-900087-0.
5. Boscolo M et al. The status of the interaction region design and machine detector interface of the FCC-ee. In: Proc. Of IPAC23. Venice. 2023. p. 7–12.
6. Raimondi P, Shatilov DN, Zobov M. arXiv:physics/0702033 [physics].
7. Boscolo M, Burkhardt H, Oide K, Sullivan MK. IR challenges and the machine detector interface at FCC-ee. Eur Phys J Plus. 2021;136(10):1068. https://doi.org/10.1140/epjp/s13360-021-02031-5.
8. Oide K et al. Design of beam optics for the future circular collider e^+e^--collider rings. Phys Rev Accel Beams. 2016;19(11):111005. https://doi.org/10.1103/PhysRevAccelBeams.19.111005.
9. von Holtey G et al. Study of beam induced particle backgrounds at the LEP detectors. Nucl Instrum Methods A. 1998;403:205.
10. Boscolo M, Bacchetta N, Benedikt M, Brunetti L, Burkhardt H, Ciarma A, Dam M, Fransesini F, Jones M, Kersevan R, et al. https://doi.org/10.18429/JACoW-IPAC2021-WEPAB029. arXiv:2105.09698 [physics.acc-ph].
11. Novokhatski A. FCC WEEK 2020. https://indico.cern.ch/event/932973/contributions/4075893/.
12. Fransesini F, Pellegrino L. Preliminary calculation for paraffin cooling system of FCC-ee IR vacuum chamber. INFN-LNF Acc. Div. Techn. Note ACCDIV-01-2023. https://da.lnf.infn.it/wp-content/uploads/sites/8/2023/04/ACCDIV-01-2023.pdf.
13. Ansys homepage. https://www.ansys.com.
14. Brochard T, Goirand L, Pasquaud J. Dispositif de raccordement entre tronçons d'anneau de synchrotron. 2016. B14959 EP, request number 17160419.2-1211/3223591 claiming priority of patent FR 16/52454.
15. Studio CST. Dassault Systemes. www.3ds.com/products-services/simulia/products/cst-studio-suite/.
16. Pancheri L et al. Fully depleted MAPS in 110-nm CMOS process with 100–300-μm active substrate. IEEE Trans Electron Devices. 2020;67(6):2393–9. https://doi.org/10.1109/TED.2020.2985639.
17. Perić I et al. High-voltage CMOS active pixel sensor. IEEE J Solid-State Circuits. 2021;56(8):2488–502. https://doi.org/10.1109/JSSC.2021.3061760.
18. Dam M. Eur Phys J Plus. 2022;137(1):81. https://doi.org/10.1140/epjp/s13360-021-02265-3. arXiv:2107.12837 [physics.ins-det].
19. https://hexagon.com/products/leica-absolute-tracker-at960-scanner-bundle.
20. Watrelot L, Sosin M, Durand S. Meas Sci Technol. 2023;34(7):075006. https://doi.org/10.1088/1361-6501/acc6e3.
21. Dannheim D, Krüger K, Levy A, Nürnberg A, Sicking E, Abusleme Hoffman AC, Parès G, Fritzsch T, Rothermund M, Jansen H, et al. https://doi.org/10.23731/CYRM-2019-001. arXiv:1905.02520 [physics.ins-det].

Publisher's Note